

Synthesis of Zeolite ZSM-5 Assisted by Di-ethanolamine and Citric Acid for the Room-Temperature Degradation of Methylene Blue Dye Using Hydrogen Peroxide as a Pro-Oxidant

I. Y. Habib

Department of Chemistry, Sa'adatu Rimi University of Education, Kano, Nigeria

Received January 9, 2024; Accepted April 5, 2024

Abstract

This study focuses on the synthesis and characterization of di-ethanolamine (DEA) and citric acid (CA) surfactant-assisted nanocrystals (NCs) of Zeolite ZSM-5, a known catalyst for hydrocarbon conversion to fuel. Chemical precipitation of $\text{NH}_4/\text{ZSM-5}$ precursor yielded spherical NCs with average sizes of 8 nm for DEA/ZSM-5 and 6 nm for CA/ZSM-5, as revealed by XRD, SEM, EDX, UV-VIS, and FTIR analyses. UV-VIS analysis demonstrated remarkable optical properties in both NCs. The catalytic performance was evaluated by degrading methylene blue (MB) dye, a model pollutant, using hydrogen peroxide (H_2O_2) as a pro-oxidant at room temperature. Both DEA/ZSM-5 and CA/ZSM-5 NCs exhibited high MB degradation efficiency (DE), increasing with higher catalyst dosages (10-50 mg). Additional H_2O_2 (2-5 mL) did not significantly affect MB degradation, possibly due to H_2O_2 's scavenging effect. The highest DEs, 96.02% for DEA/ZSM-5 and 96.06% for CA/ZSM-5, were achieved after 90 minutes, with optimized rates of 21.06×10^{-3} and $13.85 \times 10^{-3} \text{ min}^{-1}$, respectively. The degradation mechanism involves MB adsorption on the catalyst surface, followed by interaction with hydroxyl radical species (OH) to yield H_2O , CO_2 , and other mineralized products. The NCs' small sizes, improved diffusivity, strong adsorption, and favorable catalytic properties contribute to their excellent performance. Notably, the study's low energy consumption and room temperature conditions make it a cost-effective method for environmental pollutant removal.

Keywords: Zeolite ZSM-5; Diethanolamine; Citric acid; Methylene blue degradation; Hydrogen peroxide; Degradation efficiency.

1. Introduction

Zeolites are crystalline micro-porous alumino-silicate minerals with well-defined cavities and channels of molecular dimensions. The primary building units of zeolites are tetrahedra with chemical formula TO_4 ($\text{T}=\text{Al}$ or Si). They have exhibited excellent catalytic properties that is selectively used for catalyzing reactions leading to the production of aromatics, carbonylation and liquid fuels [1-4]. The potential of these catalysts come from their high surface area and a well-defined active sites and pores [5]. ZSM-5 is a classical medium pore zeolites discovered in 1965 by Mobil Company Technologies and is used in petroleum refining and petrochemicals production as both catalysts and adsorbents [6-8]. The description of the micro and meso-pores sizes of ZSM-5 were calculated in the range of about 5.4 – 5.6 Å upon analysis with a cylindrical pore model [9]. Such bigger pore sizes facilitate better ion exchange and fast diffusion of adsorbed molecules [10]. Several methods were used to synthesize ZSM-5 nanocrystals. These include hydrothermal, sol-gel based and post steaming treatment methods [10-12]. Templating agent such as tetrapropyl ammonium ion (TPA^+) was commonly used to regulate the particle size and morphology of the zeolite ZSM-5 [11-12]. Ahmadpour and Taghizadeh synthesized a mesoporous ZSM-5 with two different surfactants namely TPOAC and CTAB, which were utilized for propylene production. It was also highlighted that the ZSM-5 templated with the TPOAC was found to increase the durability and selectivity of the ZSM-5, while CTAB

templated ZSM5 do not improve durability but was emerged to have a remarkable improvement in the propylene selectivity [13]. Other improved properties as regarding the activities of these materials are acidity and porosity as compared to the properties of the conventional ZSM-5 material [10]. It has also been observed from literatures that the utilization of such templating agents in the synthesis of ZSM-5 materials could not only result to stabilization of particle sizes and morphologies but also could essentially lead to different type of morphologies. Morphologies such as spherical, hexagonal, and flaky types have been reported [5, 14-15]. Other application of surfactant could be found in the oil and gas sector as demonstrated by the utilization of non-ionic surfactant such as Enzurlan, which was used in the improvement of oil recovery in the sand T of the fields of the Ecuadorian east [16]. Specific examples of adsorbent materials other than zeolites include Biosorbent chicken feathers which was effectively used to sorb oil from sea water and waste plastic based activated carbon which was used for the treatment of tannery wastewater [17-18].

Though, it is very difficult to fabricate a morphologically controlled ZSM5 material due to the possibility of synthesizing NCs with low surface area, poor active sites and irregular morphology that could result in relatively poor physical and chemical properties. ZSM-5 has a number of properties such as thermal stability and ability to resist formation of carbonaceous deposits, which is the major problems involved in metal oxide catalysis, hence its wide application in a number of catalytic studies such as methane conversion to methanol, methanol conversion to aromatics, oxidation of chlorinated waste water pollutant such as 1,2-dichloroethane, methanol conversion to gasoline and lignin pyrolysis as well as amperometric sensor for determination of hydrazine and hydroxylamine [19-23]. Like metal oxides such as ceria and zinc oxide, ZSM-5 has also demonstrated remarkable potentials in degradation of organic pollutants such as acridine orange dye and p-nitrophenol [5, 24-26]. Other non-catalytic methods such as ultraviolet light assisted, supported with hydrogen peroxide (H_2O_2) or chlorine were also employed in pollutants degradation [27-28]. The model organic pollutant used in the present study is methylene blue (MB). MB is a formal derivative of phenothiazine and a dark green powder that yields a blue solution in water. It is used as a dye and medication. Its presence in the environment is virtually ubiquitous due to its frequent utilization in a laboratory as a redox indicator, in a textile industry as a dye and in the pharmaceuticals as drug. The aforementioned uses of MB made it a potential threat to the environment as its presence in excess causes some adverse effects such as persistent contamination and colorization of drinking and waste water among other factors, and as a consequence, its complete removal from aqueous media become necessary [29-30]. However, it has a beneficial role to play in a biomedical, pharmaceutical and medicine. Mendez et al. reported the utilization of MB in the antimicrobial photodynamic therapy in controlling the viability, vitality and the acidogenicity of dentin caries microcosms [31]. Although, its clinical application regarding the above study, has no clearly defined protocols. In the same vein Mendez et al. reported MB application in a clinical study as a promising therapeutic agent in the prevention of neuronal cell death and cognitive deficits after transient global cerebral ischaemia [31]. MB dye was found to significantly suppress the oxidative damage and expression of pro-inflammatory factors, including tumor necrosis factor- α and inter-leukin, dramatically attenuated apoptosis and neural death. In the present study, DEA/ZSM-5 and CA/ZSM-5 nanocrystals (NCs) were synthesized from NH_4 /ZSM5 through a mere modification with diethanolamine (DEA) and citric acid (CA) surfactants through chemical precipitation route, in order to investigate their reactivities and selectivities toward H_2O_2 assisted degradation of MB at room temperature.

2. Materials and methods

2.1. Synthesis of DEA/ZSM-5 and CA/ZSM-5 NCs by chemical precipitation technique

All chemicals and reagents were commercially obtained from Merck Germany and were used without further purification. Zeolite ZSM-5 ammonium powder, NH_4 /ZSM-5 with surface area of $425\text{ m}^2/\text{g}$ and $SiO_2:Al_2O_3$ ratio of 80:1 was utilized as the precursor. Surfactants used include Citric acid, CA (MF: $C_6H_8O_7$, MW:192.124 g/mol) and diethanolamine, DEA

(MF: C₄H₁₁NO₂, MW: 105.14 g/mol), nitric acid, (65% HNO₃, MW: 63.01 g/mol) and deionized water, H₂O (MF: H₂O, MW: 18.02 g/mol). In this procedure, either DEA/ZSM-5 or CA/ZSM-5 was synthesized by dissolving 0.397 g each of either CA, or DEA surfactant in 20 ml H₂O and 2g of NH₄/ZSM-5 was subsequently added to form an aqueous solution. Upon magnetic stirring at room temperature, RT, 3 drops of (65% HNO₃/H₂O, v/v, 1:1) was added in order to achieve the desired pH. The recorded pH of the solutions were 9.75 and 2.38 for DEA and CA, respectively. Reaction mixtures were allowed to stand for 24 h under vigorous magnetic stirring at 70°C. The slurry was then centrifuged several times at 7000 rpm in RT for 10 min and then finally calcined at 500°C for 4 h.

2.2. Sample preparation for degradation studies

Materials used include; methylene blue dye, MB (MF: C₁₆H₁₈ClN₃S, MW 319.85 g/mol), hydrogen peroxide (MF: H₂O₂, MW 34.0147 g/mol), de-ionized water (MF: H₂O, MW: 18.02 g/mol), DEA/ZSM-5 and CA/ZSM-5. The preparation procedure used in this study was similar to that used in our previously reported literature [32-33]. Precisely 10 and 50 mg of either DEA/ZSM-5 or CA/ZSM-5 NCs was introduced into a 250 ml beaker containing 100 mL of 10 mg/L MB aqueous solution with about 2 or 5 ml of (30 % H₂O₂ solution). The solution mixture was then covered with a para-film to prevent direct light and air interaction. Solution pH was recorded to be 5.8. The reaction takes place in a fume hood on a digital hot plate under a vigorous magnetic stirring at RT for a period of 5 - 120 min. The reaction is said to be continuous within the specified reaction time while sample (about 5 ml) was taken without stopping the reaction across the specified time intervals until the last sample was taken. Samples were subsequently centrifuged at 3000 rpm for 15 min before UV-Vis analysis. The degradation efficiencies of the MB were calculated based on the formula reported by Li et al. as shown in equation (1) [34].

$$D (\%) = \frac{A_0 - A}{A_0} \times 100 \quad [1]$$

where D stands for the degradation efficiency; A₀ stands for the initial concentration of MB absorption before reaction; and A, is the MB concentration at time, t.

2.3. Nanocrystals characterizations

The X-ray diffractions were carried out for both DEA/ZSM-5 and CA/ZSM-5 NCs with a Shimadzu X-ray diffractometer (XRD-7000), which was programmed with a step of 0.021 using Cu K α radiation ($\lambda = 1.54060 \text{ \AA}$) to investigate the structural properties of the nanocrystalline powders. The X-ray irradiation took place at 2θ range between 5-70°, under 5°/min. The morphology and the average particle diameter were determined using the field emission scanning electron microscope (FE-SEM) JSM-7610F, while the chemical compositions of the prepared samples were determined using the energy dispersive X-ray spectroscopy (EDX). The ultraviolet-visible range (200 - 800 nm) of the electromagnetic radiation of the Cary 500 UV-VIS-NIR Spectrophotometer was used to determine the optical absorption of the prepared films at room temperature. The symmetric and asymmetric stretching vibrations of the TO₄, SiO₄ and AlO₄ tetrahedron in the ZSM-5 framework were investigated using the Attenuated Total Reflectance (ATR) accessory of the Fourier transform infrared spectrophotometer (FTIR).

3. Results and discussion

3.1. XRD analysis

The structure of the DEA/ZSM5 and CA/ZSM5 NCs were investigated using X-ray diffraction. The diffraction patterns for the materials are depicted in Fig. 1. It is clearly seen that the formation of a well crystalline peaks at the 2θ positions (9.3, 10.1, 23.2, 23.7 and 24.2°) implies the formation of MFI zeolite framework type with JCPDS NO. 00-037-0359 [5-12]. These peaks correspond to the following reflection planes ((011), (200), (051), (033) and (133)) as reported from literature [35]. Based on the sharpness of the above peaks, the synthesized materials could be regarded as crystallines. Both DEA/ZSM5 and CA/ZSM5 NCs exhibit similar

XRD patterns with the complete absence of secondary phase due to impurities or from incomplete removal of DEA and CA residues during calcination. Similar XRD patterns have been reported from literatures [10,15]. The average crystallite size of the NCs were estimated using Scherrer equation while utilizing the XRD data of the three close peaks mentioned in the diffractograms [36]. The recorded values for the average crystallite sizes for the DEA/ZSM-5 and CA/ZSM-5 are 23 and 25 nm, respectively.

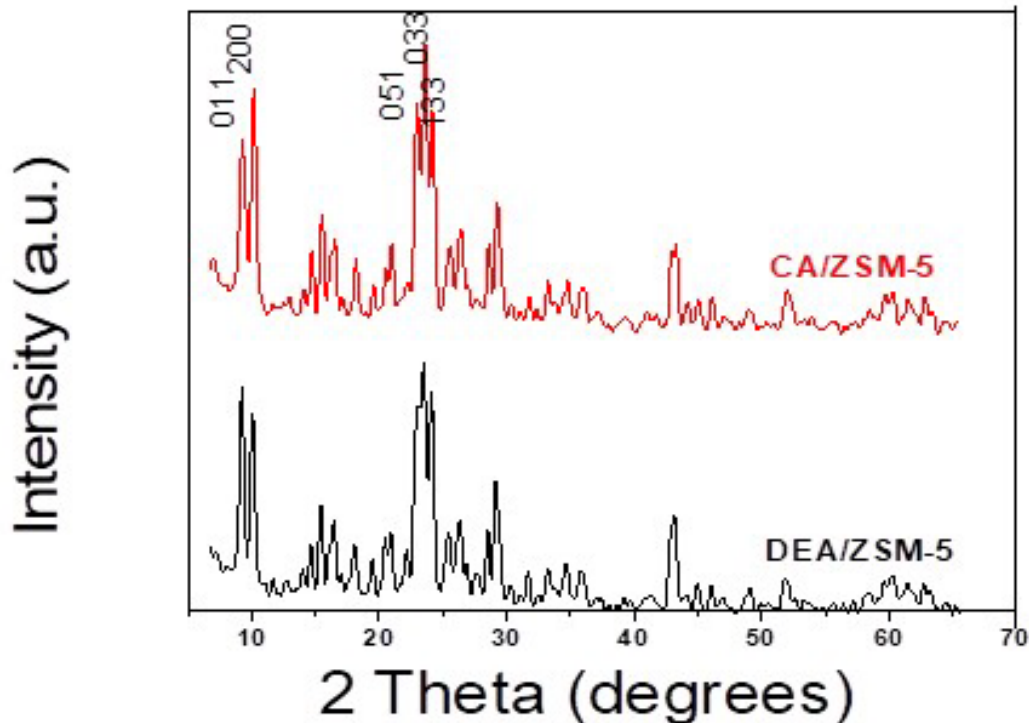


Figure 1. XRD patterns for the DEA/ZSM5 and CA/ZSM5 NCs.

3.2. SEM analysis

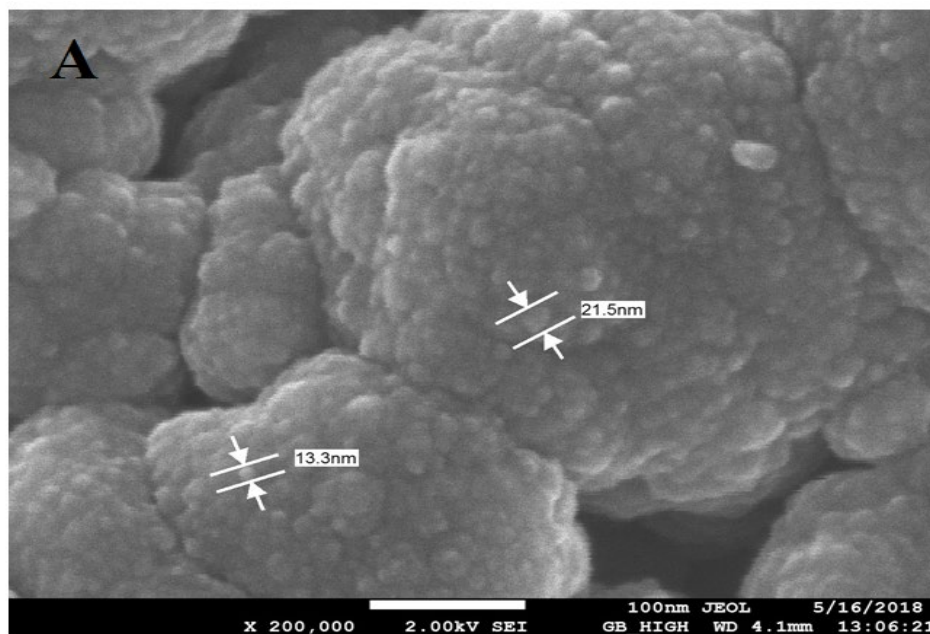


Figure 2. SEM images of the (A) DEA/ZSM-5

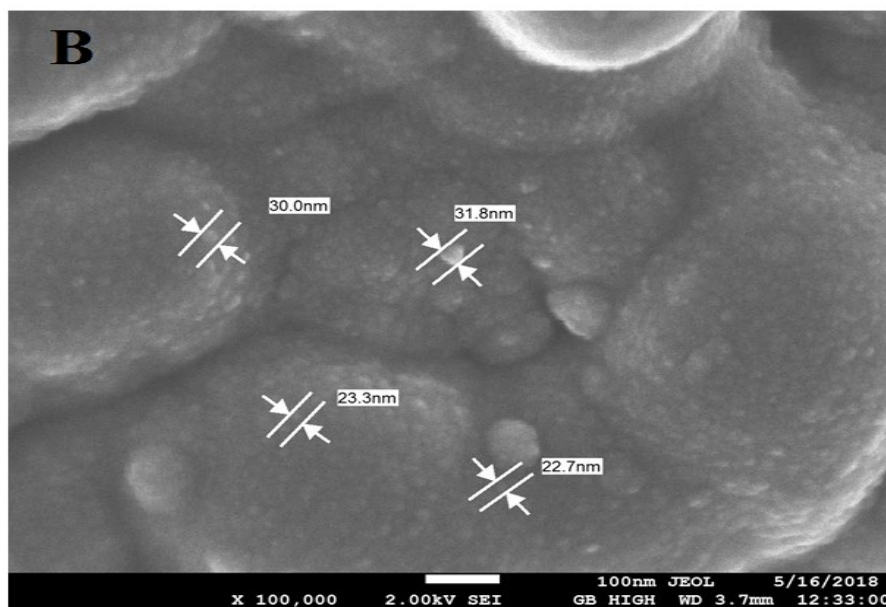


Figure 2. SEM images of the (B) CA/ZSM-5

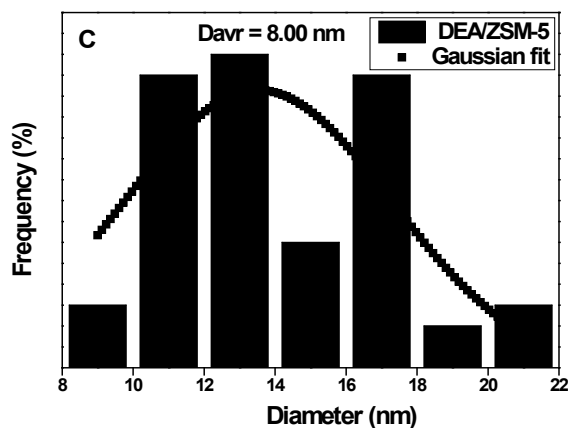
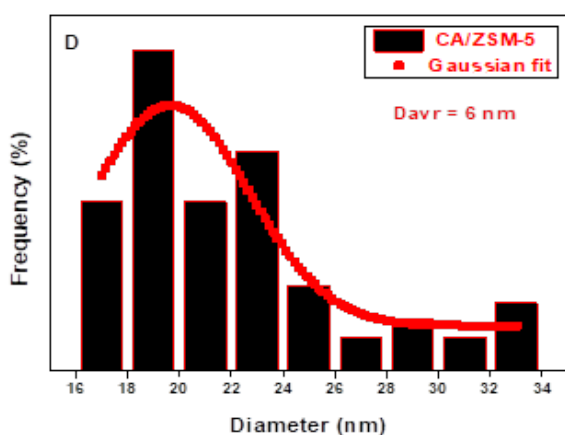


Figure 2. Diameter distribution of the (C) DEA/ZSM-5.

Figure 2. Diameter distribution of the (D) CA/ZSM-5.

The SEM analysis was carried out using a field emission scanning electron microscope (FE-SEM) to determine the particles sizes and morphologies of the DEA/ZSM-5 and CA/ZSM-5 NCs. The SEM analysis were done using 100 nm scale under high magnifications as shown in Fig. 2 (A and B). It could be seen that the SEM images consist of a spherical morphologies and a uniform distribution of particles as shown in Fig. 2 (A and B). Similar spherical morphology exhibited by zeolite ZSM-5 was also reported from literatures [12,14]. Statistical analysis of these particles are carried out to ensure accurate estimation of the actual particle size. The statistical distribution is analyzed using particles from the SEM micrographs. A nonlinear plot was employed to illustrate the particle size distribution using Gaussian fitting as shown in Fig. 2 (C and D). The recorded average particle size of the DEA/ZSM-5 and CA/ZSM-5 NCs are 8 and 6 nm, respectively, as shown in Fig. 2 (C and D). It is also noted that few particles interact to form agglomerates, though the concentration of the agglomerate is very few, indicating that the force of repulsion between the particles outweigh the corresponding force of attraction. Thus, suggesting that, both DEA and CA could be used as suitable surfactants for controlling both size and inter-particles agglomeration in ZSM-5 material.

3.3. EDX analysis

The energy dispersive X-ray spectroscopy (EDX) was used to determine the chemical compositions and their respective percentages of the chemical constituents in the DEA/ZSM-5 and CA/ZSM-5 NCs are also recorded. Fig. 2 (A and B), present the spectra showing the percentage chemical compositions of the DEA/ZSM-5 and CA/ZSM-5 NCs. The spectra clearly show the percentage elemental composition of the O, Al, Si, and C, which are the main building blocks of a typical zeolite ZSM-5 material except for C as shown in Fig. 2 (A and B). The C impurity came from the coating materials.

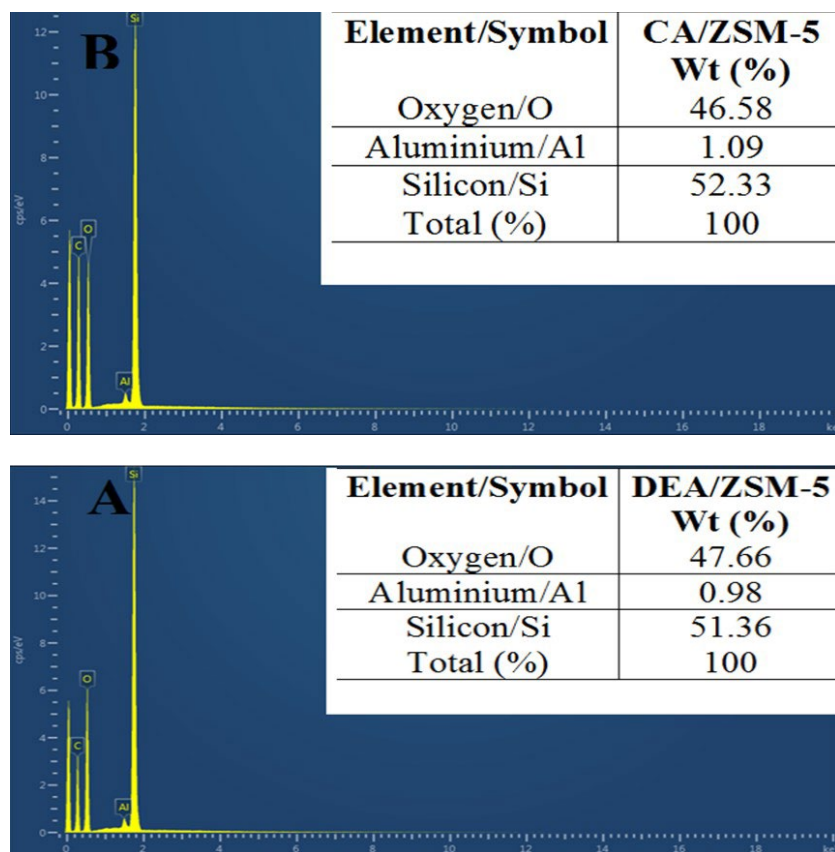


Figure 3. The EDX spectrum of the (A) DEA/ZSM-5 and; (B) CA/ZSM-5.

3.4. UV-VIS analysis

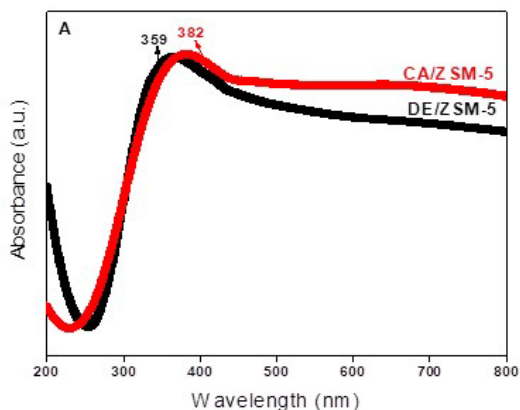


Figure 4 Absorption spectra for DEA/ZSM-5 and CA/ZSM-5.

The UV-Vis absorption of the samples were conducted to determine the optical absorptions of the samples. Fig. 3 shows the absorption spectra of the samples. This absorption was found out to occur below 400 nm. The wavelengths of the absorptions were found o to be 359 and 382 nm recorded for DEA/ZSM-5 and CA/ZSM-5 NCs, respectively. This shows that, these NCs have excellent optical properties, which could be used to carry out a number of electronic applications such as such as phenolic sensor and photocatalysis [26, 37].

3.5. FTIR analysis

The infrared absorptions of NCs were conducted with the Fourier transform infrared spectroscopy (FTIR) to uncover the symmetric and asymmetric stretching vibrations due to TO_4 , SiO_4 and AlO_4 tetrahedron in the ZSM-5 framework across 4000 - 400 cm^{-1} range. The FTIR transmittance spectra is depicted on Fig. 5.

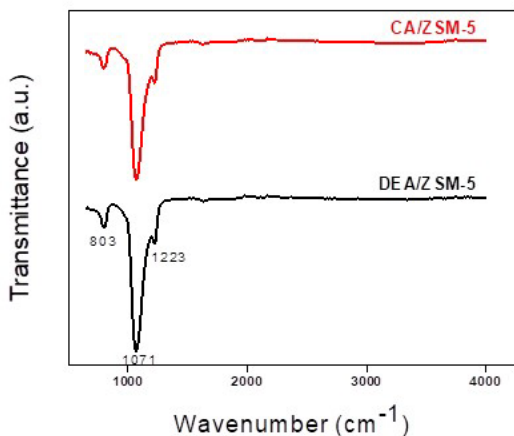


Figure 5. FTIR transmittance spectra for DEA/ZSM-5 and CA/ZSM-5.

It could be seen that only few anticipated bands of equal intensities were detected for both DEA/ZSM-5 and CA/ZSM-5 NCs, indicating the occurrence of a complete absence of impurity, which is well correlated with the XRD diffractograms recorded in this study. The recorded absorption bands include a weak band at 804 cm^{-1} , a strong band at 1071 cm^{-1} and a shoulder at 1223 cm^{-1} . The weak band at 804 cm^{-1} , is due to symmetric stretching vibration, while strong band at 1071 cm^{-1} , is due to TO_4 asymmetric stretching vibrations and band at 1223 cm^{-1} , is due to external asymmetry of SiO_4 and AlO_4 tetrahedron in the ZSM-5 framework [26, 37]. The position of absorption bands in both samples were found to be similar, indicating that, both the materials emanate from the same origin.

4.1. Methylene blue degradation study for DEA/ZSM-5 NCs

Figure 6 (a-d) display the absorption spectrum showing the degradation sequence of the MB as a function of time using DEA/ZSM-5 NCs. Samples analyses were done using UV-Vis-NIR spectrometer at 200 - 800 nm. All samples show a remarkable absorption at λ_{max} 665 nm, which is in agreement with the existing literature [24]. This band at 665 nm is thus, correlated with the chromophore of the MB. Since the intermediate of the reaction cannot be determined from the absorption curves, therefore, the subsequent decrease in the intensity of the MB absorption peaks indicate decolorization and gradual reduction of the MB concentration. This phenomenon could lead to the gradual decomposition of benzene-like structures to carbon dioxide and water through mineralization [38]. Absorbance values and peak intensities decrease with the reaction time but more decreasing with increasing concentration of H_2O_2 from 2 ml to 5 ml as shown in Fig. 6 (A-D). As the DEA/ZSM-5 dosage increases from 10 mg to 50 mg, the absorption peaks decreased rapidly with increasing reaction time and the highest peak intensity decreases upon the addition of 2 ml H_2O_2 at 50 mg catalyst dosage. The plot of the MB degradation efficiencies of DEA/ZSM-5 NCs is depicted in Fig. 6 (E).

4.2. Methylene blue degradation study for CA/ZSM-5 NCs

Similarly, the CA/ZSM-5 degradation absorption spectra is also presented in Fig. 7 (A-D). From the above figures, it could be seen that, the absorption λ_{max} of 665 nm as well as the successive degradation of MB dye was successful. It is also interesting to report that the CA/ZSM-5 MB degradation trend is homologous to that of DEA/ZSM-5. The plot of the MB degradation efficiencies of CA/ZSM-5 NCs is depicted in Fig. 7 (E). The DEA/ZSM-5 and CA/ZSM-5 NCs catalytic performances are best demonstrated using the degradation efficiency parameter. It is shown in Fig. 7(E) that the DEA/ZSM-5 NCs recorded its highest values at the highest reaction time (120 min) leading to degradation efficiencies of 60.78, 45.10, 99.02, and 95.10 %, which were carried out at 10 mg (2 ml H_2O_2), 10 mg (5 ml H_2O_2), 50 mg (2 ml H_2O_2) and 50 mg (5 ml H_2O_2), respectively, as shown in Fig. 6 (E). Similarly, the highest recorded values for degradation efficiencies of CA/ZSM-5 NCs are 67.92, 46.23, 99.06, and 95.28 %, which were also carried out at the same conditions recorded for DEA/ZSM-5 NCs as depicted in Fig. 7 (E).

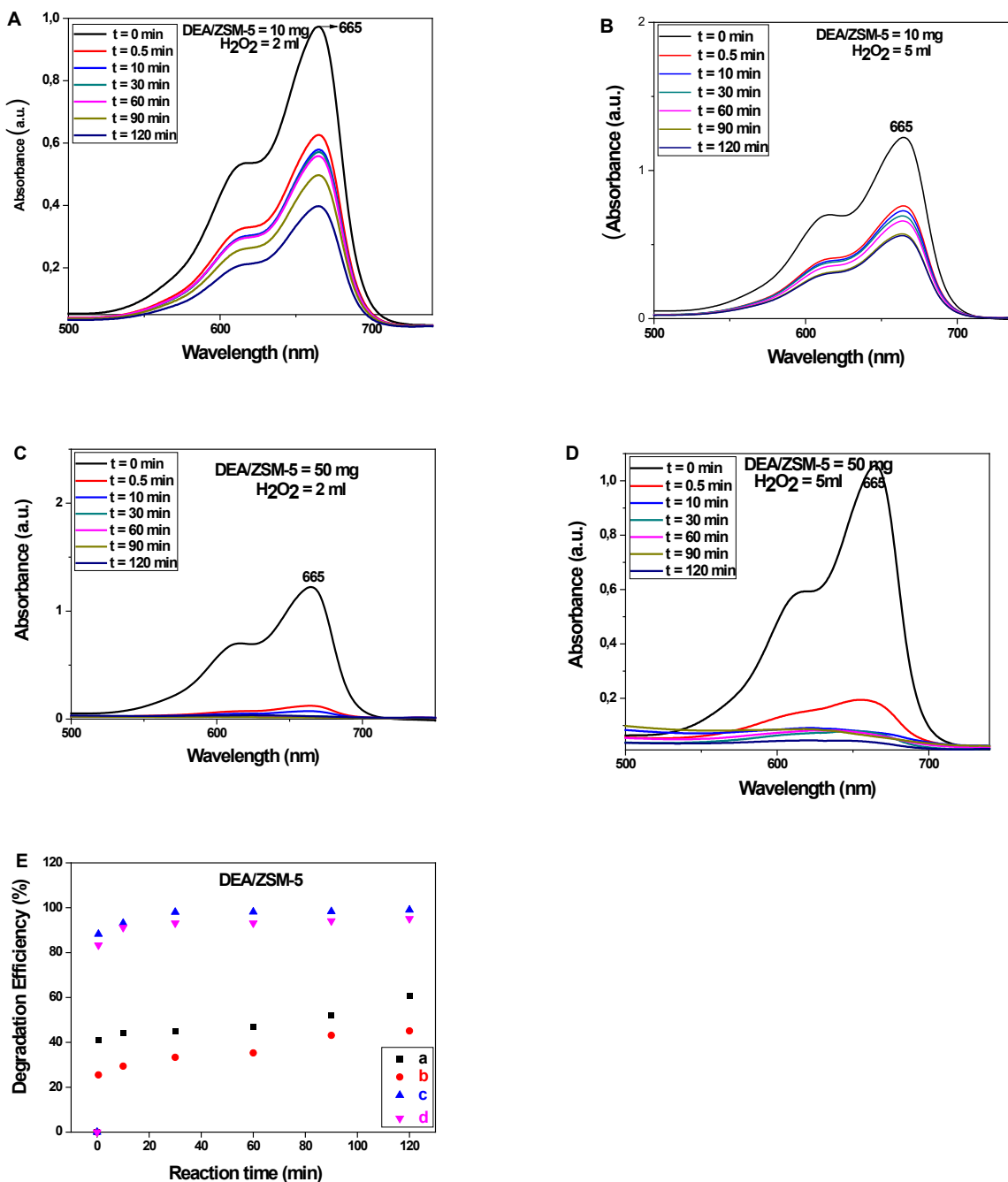


Figure 6. MB degradation absorption spectra for: (A) 10 mg DEA/ZSM-5 with 2 ml H₂O₂ (B) 10 mg DEA/ZSM-5 with 5 ml H₂O₂ (C) 50 mg DEA/ZSM-5 with 2 ml H₂O₂ (D) 50 mg DEA/ZSM-5 with 5 ml H₂O₂ (E) Degradation efficiencies of MB at different reaction conditions; (a) 10 mg DEA/ZSM-5 with 2ml H₂O₂ (b) 10 mg DEA/ZSM-5 with 5ml H₂O₂ (c) 50 mg DEA/ZSM-5with 2ml H₂O₂ (d) 50 mg DEA/ZSM-5 with 5ml H₂O₂.

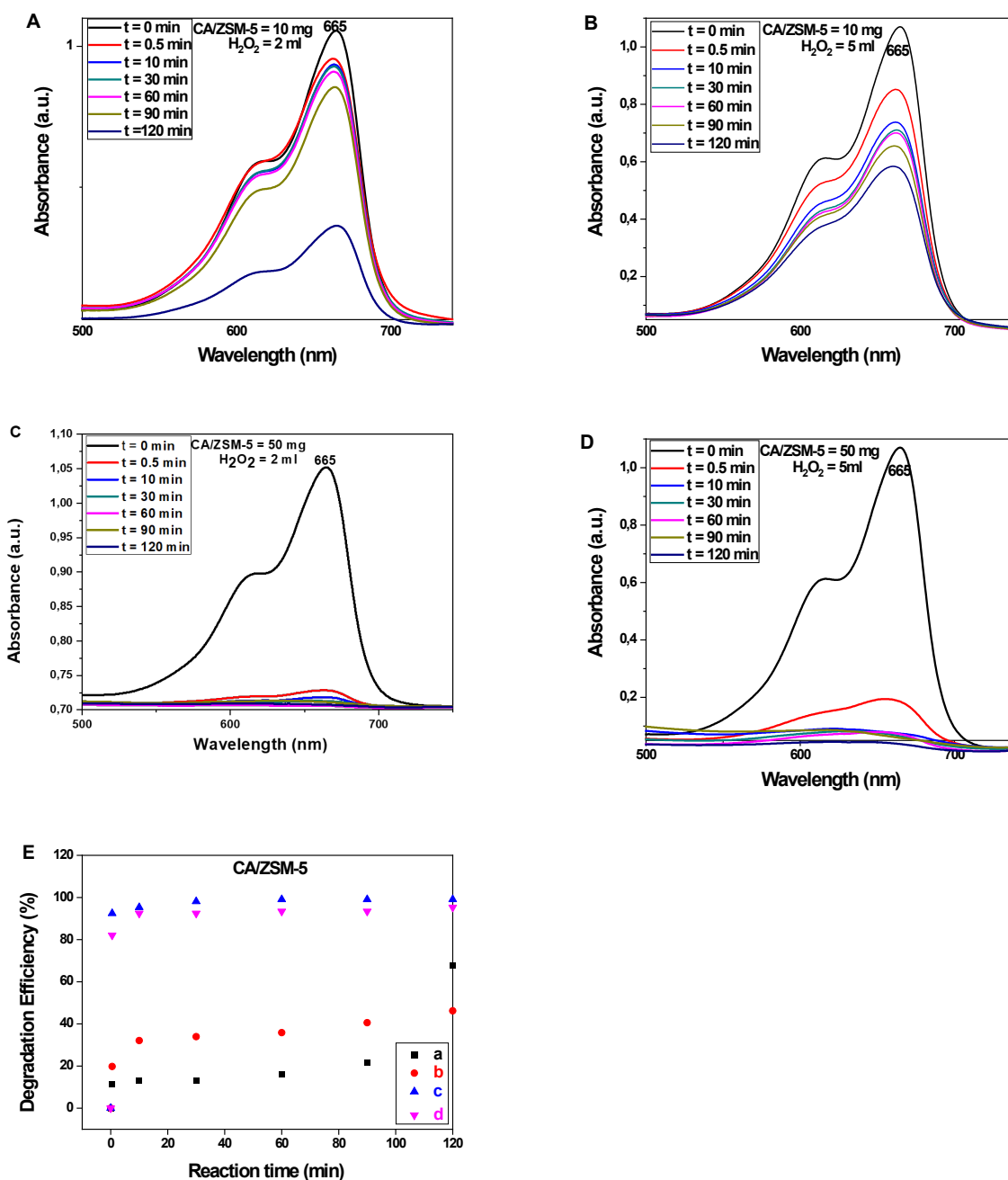
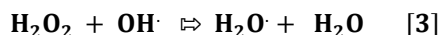


Figure 7. MB degradation absorption spectra for: (A) 10 mg CA/ZSM-5 with 2 ml H₂O₂ (B) 10 mg CA/ZSM-5 with 5 ml H₂O₂ (C) 50 mg CA/ZSM-5 with 2 ml H₂O₂ (D) 50 mg CA/ZSM-5 with 5 ml H₂O₂ (E) Degradation efficiencies of MB at different reaction conditions; (a) 10 mg CA/ZSM-5 with 2 ml H₂O₂ (b) 10 mg CA/ZSM-5 with 5 ml H₂O₂ (c) 50 mg CA/ZSM-5 with 2 ml H₂O₂ (d) 50 mg CA/ZSM-5 with 5 ml H₂O₂.

From the results presented above, it could be observed that the higher values for the degradation efficiencies were only achieved upon increasing the catalyst amounts from 10 mg to 50 mg in both catalysts reaction media, whereas increasing the amount of H₂O₂ from 2 mL to 5 mL do not show much significant effect. These high degradation values indicate the excellent reactivity, selectivity as well as robustness of the DEA/ZSM-5 and CA/ZSM-5 catalysts. Based on the DE values recorded for the DEA/ZSM-5 and CA/ZSM-5 NCs, the two different catalysts

yield similar result. Hence, DEA and CA surfactants do not have any significant effect in tuning the catalytic activity of the ZSM-5 material, rather than controlling size and preventing inter-particles agglomeration. The main rationale behind the decrease in the MB degradation in the presence of excess H₂O₂ (5 mL) in the reaction medium could be attributed to the scavenging effect of H₂O₂. This phenomenon decreases significantly the amount of generated species such as hydroxyl radical ($\cdot\text{OH}$) in the reaction medium. This is because only the optimum amount of H₂O₂ was meant to oxidize organic molecules effectively. This argument could be verified from the work of Modal *et al.* on the degradation of ciprofloxacin according to the following equation [39].



One of the most probable and effective radical species for degrading organic pollutants from aqueous solution was found to be $\cdot\text{OH}$ as reported from literature [24,40-41]. Details on the scavenging studies of the $\cdot\text{OH}$ using an alcohol based scavenger could be found in the previously reported literature [24]. Li *et al.* also reported the potential of DMSO in $\cdot\text{OH}$ suppression effects during their oxidation study in the presence of excess H₂O₂ [34]. By analogy, DMSO may also serve as a scavenger for retarding the reactivity of the generated $\cdot\text{OH}$ radical species in a reaction medium. Hara *et al.* also reported the scavenging effect of dissolved CO₂ during benzene degradation [42]. In order to explore further to identifying other different reactive species that could certainly establish suitable mechanisms of organic pollutants degradation in drinking or waste water systems, Li *et al.* also reported other scavengers such as ascorbic acid, t-butanol, sodium azide, benzoquinone, and tiron in their quest for investigating the type of reactive species such as singlet oxygen, hydroxyl and superoxide radical species that may be present in the reaction media [43]. As further highlighted by Li *et al.*, sodium azide is regarded as a popular scavenger for singlet oxygen, whereas t-butanol is used to scavenge hydroxyl radical, while benzoquinone, ascorbic acid and tiron are the scavengers employed for removing superoxide radical species. Upon utilization of all the aforementioned scavengers in the contaminant degradation, they found out that, only t-butanol and sodium azide were found to have significantly degraded the organic pollutants in the reaction media indicating the presence of only hydroxyl radical and singlet oxygen in the system. This shows that superoxide radical in the reaction media is either dormant or completely not available. Rivas *al.* reported the presence of singlet oxygen as an active specie in their organic pollutants degradation studies [21]. Despite the participation of other reactive species such as superoxide radical and singlet oxygen species in the organic pollutants degradation processes, hydroxyl radical is considered the most influential due to its non-selective pollutants degradation potential to the corresponding CO₂ and H₂O molecules, the major products of complete mineralization [21]. The DEA/ZSM-5 and CA/ZSM-5 NCs catalytic trends explain the complete dependency of the MB degradation on the catalyst dosage rather than the amount of H₂O₂ used in the reaction media.

4.3. The rate and methylene blue degradation mechanism

Both DEA/ZSM-5 and CA/ZSM-5 NCs as heterogeneous catalysts have been used to investigate the degradation as well as the kinetics of the H₂O₂ catalytic oxidation process with MB as the model organic pollutant. As shown in Fig. 6 (E) and 7 (E), DEA/ZSM-5 and CA/ZSM-5 NCs demonstrated excellent catalytic degradation activities at all reaction times and the highest degradation took place at 50 mg dosage and 2 mL H₂O₂ at 120 min. The kinetic plots for the degradation of MB is demonstrated in Fig. 8 (A and B). The plot of pseudo first order could be obtained from the slope of the straight line through the plot of $\ln(\text{MB})$ as a function of time (min) as shown in Fig. 8 (A and B). The resulting pseudo first order rate constant (k) values are 3.60×10^{-3} , 2.84×10^{-3} , 21.06×10^{-3} and $16.35 \times 10^{-3} \text{ min}^{-1}$ for DEA/ZSM-5 and 7.71×10^{-3} , 3.32×10^{-3} , 13.85×10^{-3} and $15.56 \times 10^{-3} \text{ min}^{-1}$ for CA/ZSM-5, which correspond to the 10 mg (2 mL H₂O₂), 10 mg (5 mL H₂O₂), 50 mg (2 mL H₂O₂) and 50 mg (5 mL H₂O₂) in either DEA/ZSM-5 or CA/ZSM5 NCs, respectively as shown in Fig. 8 (C). It is obvious that the rate constant, $k = 0.027$ and 0.02 , which corresponds to the 50 mg (2 mL H₂O₂) dosage utilized for DEA/ZSM-5 and CA/ZSM-5 respectively, appeared to be higher, which correlates with the optimized condition towards the MB catalytic degradation. The schematic for the MB

and ZSM-5 structure as well as mineralization process is illustrated in a scheme depicted in Fig. 8 (D). This scheme demonstrates the process of mineralization using MB as the model pollutant and a hypothetical ZSM-5 structure. It is also important to note that degradation is an oxidation process that requires an oxygen source for the completion of the reaction. In this study, H_2O_2 was used as the pro-oxidant and DEA/ZSM-5 or CA/ZSM-5 NCs was used as the oxidant activator for the oxidation reaction to occur. From the above scheme, it could be observed that the oxidation reaction occurs at the surface of the ZSM-5 catalyst through a process known as adsorption. It also summarizes chemically, the process of catalytic degradation of MB pollutant. The MB degradation was facilitated by the generation of $\cdot\text{OH}$ radical in the reaction medium. During the adsorption-desorption process, the $\cdot\text{OH}$ radical interact strongly with the MB molecules, leading to the opening of the complex ring of MB structure, and in consequence, resulting to a complete mineralization of the MB molecules. The above experimental results signify that these catalysts, DEA/ZSM-5 and CA/ZSM-5 NCs, could be applied in various advanced oxidation processes as excellent catalysts for the decolorization, degradation, disinfection, decontamination and subsequently removal of organic pollutants particularly MB from aqueous media such as wastewater or drinking water.

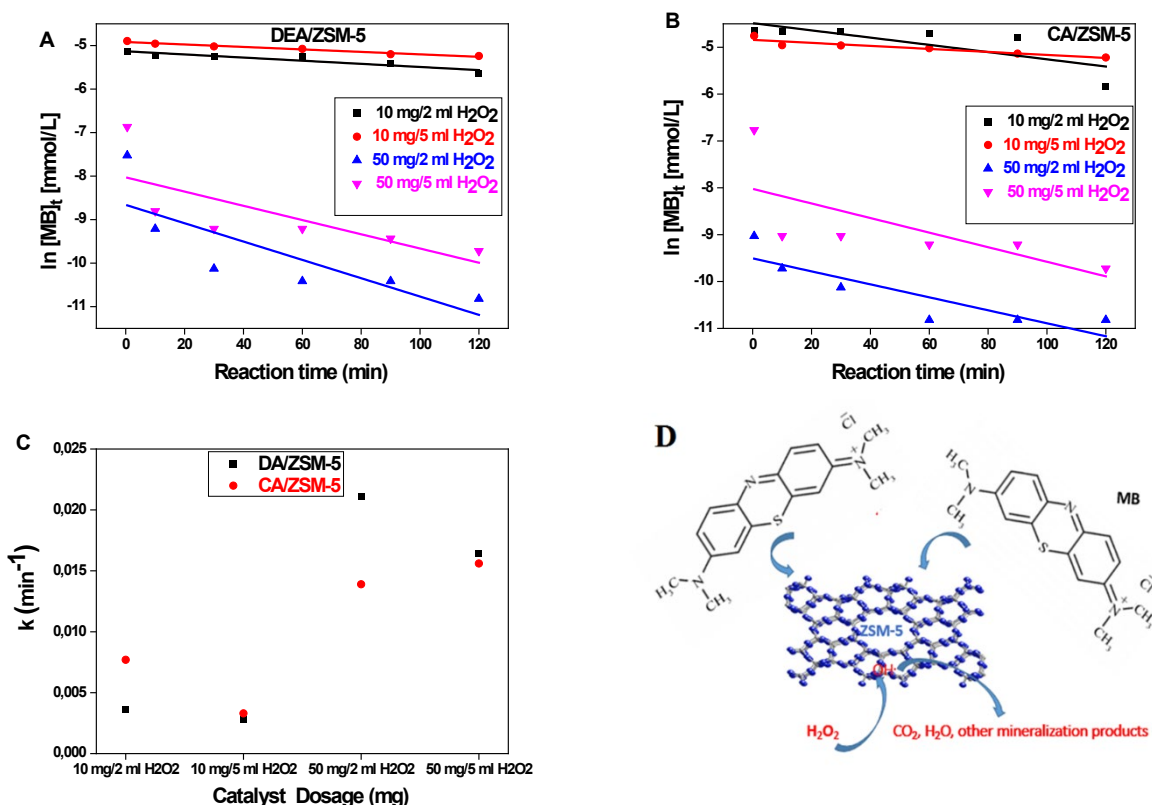


Figure 8. Linear fittings of the $\ln [\text{MB}]_t$ vs. reaction time at different catalyst dosage and H_2O_2 concentrations for (A) DEA/ZSM-5 (B) CA/ZSM-5 and; (C) The plot of k vs. catalyst composition for the DEA/ZSM-5 and CA/ZSM-5. (D) Schematic of the MB adsorption on ZSM-5 surface.

5. Conclusion

This study achieved the successful synthesis of modified zeolite ZSM-5 nanocrystals (NCs) using di-ethanolamine (DEA) and citric acid (CA) as surfactants via a chemical precipitation technique. Rigorous characterization methods, including XRD, FE-SEM, EDX, UV-Vis-NIR, and FTIR, confirmed the formation of MFI type zeolite with well-defined peaks and an absence of impurities. FE-SEM images depicted uniformly spherical grains, revealing small grain sizes of approximately 8 nm for DEA/ZSM-5 and 6 nm for CA/ZSM-5 NCs. UV-Vis absorption spectra

exhibited distinct absorption peaks at 359 nm for DEA/ZSM-5 and 382 nm for CA/ZSM-5, showcasing strong light absorption capabilities.

Utilizing DEA/ZSM-5 and CA/ZSM-5 as heterogeneous catalysts for methylene blue (MB) degradation with hydrogen peroxide (H_2O_2) proved successful. MB absorption occurred at λ_{max} of 664 nm, consistent with prior literature. Degradation efficiencies (DE) increased with higher catalyst dosages (10 mg to 50 mg), with H_2O_2 quantity (2 mL to 5 mL) having a less pronounced effect due to its scavenging effect.

DEA and CA emerged as effective surfactants, controlling particle size and preventing agglomeration in ZSM-5 materials. Both catalysts demonstrated excellent DE values, affirming ZSM-5's selectivity, suitability, and stability for MB dye degradation in aqueous solutions. The optimal reaction time for achieving the highest DE values was identified as 90 minutes.

The degradation mechanism involved MB adsorption on the catalyst surface, followed by interaction between hydroxyl radical species and MB molecules, yielding H_2O , CO_2 , and other mineralized products. In summary, this study showcased the successful synthesis and characterization of DEA/ZSM-5 and CA/ZSM-5 NCs, highlighting their efficacy as catalysts for MB degradation. These catalysts present promising applications in wastewater treatment and environmental remediation, given their robust catalytic performance.

References

- [1] Hassanpour J, Zamani M, Dabbagh HA. Effect of ketene additive and Si/Al ratio on the reaction of methanol over HZSM-5 catalysts: Effect of ketene on MTG. *Appl. Organometal. Chem.*, 2017; 1-10.
- [2] Zheng Y, Wang F, Yang X, Huang Y, Liu C, Zheng Z. Study on aromatics production via the catalytic pyrolysis vapor upgrading of biomass using metal-loaded modified H-ZSM-5. *J. Anal. Appl. Pyrolysis*, 2017; 126: 169–179.
- [3] Wong SL, Ngadi N, Abdullah TAT, Inuwa IM. Conversion of low density polyethylene (LDPE) over ZSM-5 zeolite to liquid fuel. *Fuel*, 2017; 192: 71–82.
- [4] Celik FE, Kim T, Bell AT. Effect of zeolite framework type and Si/Al ratio on dimethoxymethane carbonylation. *J. Catal.*, 2010; 270(1): 185–195.
- [5] Abdolraouf SKH, Samadi-Maybodi A, Ghobakhlou M. Synthesis and characterization of modified ZSM-5 nanozeolite and their applications in adsorption of Acridine Orange dye from aqueous solution. *J. Porous Materials*, 2013; 20(4): 909–916.
- [6] Teh LP, Triwahyono S, Jalil AA, Mukti RR, Aziz MAA, Shishido T. Mesoporous ZSM5 having both intrinsic acidic and basic sites for cracking and methanation. *Chem. Eng. J.*, 2015; 270: 196–204.
- [7] De Rivas B, Sampedro C, López-Fonseca R, Gutiérrez-Ortiz MÁ, Gutiérrez-Ortiz JI. Low-temperature combustion of chlorinated hydrocarbons over $\text{CeO}_2/\text{H-ZSM5}$ catalysts. *Appl. Catal. A Gen.*, 2012; 417–418: 93–101.
- [8] Hu Y, Jiang Z, Xu C, Mei T, Guo J, Tim W. Monodisperse ZnO Nanodots: Synthesis, characterization, and optoelectronic properties. *J. Phys. Chem. C.*, 2007; 111: 9757–9760.
- [9] Al-Dughaiter AS, De Lasa H. HZSM-5 Zeolites with Different $\text{SiO}_2/\text{Al}_2\text{O}_3$ Ratios. Characterization and NH_3 Desorption Kinetics. *Ind. Eng. Chem. Res.*, 2014; 53(40): 15303–15316.
- [10] Wang Y, Yang D, Li S, Chen M, Guo L, Zhou J. Ru/hierarchical HZSM-5 zeolite as efficient bifunctional adsorbent/catalyst for bulky aromatic VOCs elimination. *Microporous Mesoporous Mater.*, 2018; 258: 17–25.
- [11] Rostamizadeh M, Yaripour F. Bifunctional and bimetallic Fe/ZSM-5 nanocatalysts for methanol to olefin reaction. *Fuel*, 2016; 181: 537–546.
- [12] Soltanali S, Halladj R, Rashidi A, Bazmi M. Mixed templates application in ZSM-5 nanoparticles synthesis: Effect on the size, crystallinity, and surface area. *Adv. Powder Technol.*, 2014; 25(6): 1767–1771.
- [13] Ahmadpour J, Taghizadeh M. Catalytic conversion of methanol to propylene over high-silica mesoporous ZSM-5 zeolites prepared by different combinations of mesogenous templates. *J. Nat. Gas Sci. Eng.*, 2015; 23: 184–194.
- [14] Liu P, Jin L, Jin C, Zhang J, Bian S. Synthesis of hierarchically porous silicate-1 and ZSM-5 by hydrothermal transformation of SiO_2 colloid crystal/carbon composites. *Microporous Mesoporous Mater.*, 2018; 262: 217–226.

- [15] Liu Y, Zhao M, Cheng L, Yang J, Liu L, Wang J, Yin D, Lu J, Zhang Y. Facile synthesis and its high catalytic performance of hierarchical ZSM-5 zeolite from economical bulk silicon oxides. *Microporous Mesoporous Mater.*, 2018; 260: 116–124.
- [16] Gavilanes J, Gómez F, Cerón G, & Valencia R. Analysis of the Injection of Non-Ionic Surfactant in Cores of a Mature Field to Increase the Recovery Factor. *Pet Coal*, 2023; 65(1): 194-208.
- [17] Ayad, M. A., Aboul-Fetouh, M. E., Mohamed, S. Z., Abdallah, R. I., & Aboul-Fotouh, T. M. Application of Renewable Biosorbent Material in Water Treatment from Oil Pollution. *Pet Coal*, 2023; 65(4): 1168-1179.
- [18] Hmood, A. M., Al Sahbooni, A., & Ahmed, S. R. Treatment of Refinery Wastewater by a Waste Plastic based Activated Carbon. *Pet Coal*, 2023; 65(4): 1153-1167.
- [19] Krisnandi YK, Yusri S, Gotama HS, Octaviani S, Sihombing R. Synthesis and Characterization of Hierarchical Co/ZSM-5 as Catalyst for Methane Partial Oxidation. *Int. J. Environ. Bioener.*, 2012; 3(2): 121-131.
- [20] Jia Y, Wang J, Zhang K, Feng W, Liu S. Nanocrystallite self-assembled hierarchical ZSM-5 zeolite microsphere for methanol to aromatics. *Microporous Mesoporous Mater.*, 2017; 47: 03–115.
- [21] De Rivas B, et al. Influence of the synthesis route on the catalytic oxidation of 1,2-dichloroethane over CeO₂/H-ZSM5 catalysts. *Appl. Catal. A Gen.*, 2013; 56: 6–104.
- [22] C JA, et al. Modification of natural clinoptilolite and ZSM-5 with different oxides and a study of the obtained products in lignin pyrolysis. 2015; 0(5): 17–729.
- [23] Rostami S, Azizi SN, Ghasemi S. Simultaneous electrochemical determination of hydrazine and hydroxylamine by CuO doped in ZSM-5 nanoparticles as a new amperometric sensor. *New J. Chem.*, 2017; 1: 13712-13723.
- [24] Habib IY, Muhammad M, Yakasai MY, Abdullahi AD. Structural, morphological and optical properties of Ni-doped CeO₂ nanospheres prepared by surfactant free co-precipitation technique. *Open J. of Sci. and Tech.*, 2021; 4(4): 165-77.
- [25] Zulmajdi SLN, Ajak SNFH, Hogley J, Duraman N, Harunsani MH. Kinetics of Photocatalytic Degradation of Methylene Blue in Aqueous Dispersions of TiO₂ Nanoparticles under UV-LED Irradiation. *American Journal of Nanomaterials*, 2017; 5(1): 1–6.
- [26] Ali I, Hassan A, Shabaan S, El-Nasser K. Synthesis and characterization of composite catalysts Cr/ZSM-5 and their effects toward photocatalytic degradation of p-nitrophenol. *Arab. J. Chem.*, 2017; 10: S2106–S2114.
- [27] Bensalah N, Bedoui A. Efficient degradation of tannic acid in water by UV/H₂O₂ process. *Sustain. Environ. Res.* 2018 ; 28(1): 1–11.
- [28] Wu Z, Guo K, Fang J, Yang X, Xiao H, Hou S. Factors affecting the roles of reactive species in the degradation of micropollutants by the UV/chlorine process. *Water Res.*, 2017; 126: 351–360.
- [29] Khaksar M, Amini M, Boghaei DM, Chae KH, Gautam S. Mn-doped ZrO₂ nanoparticles as an efficient catalyst for green oxidative degradation of methylene blue. *Catal. Commun.*, 2015; 72(3): 1–5.
- [30] Safardoust-Hojaghan H, Salavati-Niasari M. Degradation of methylene blue as a pollutant with N-doped graphene quantum dot/titanium dioxide nanocomposite. *J. Clean. Prod.*, 2017; 148: 31–36.
- [31] Mendez DAC, Gutierrez E, Dionísio EJ, Oliveira TM, Buzalaf MAR, Rios D, Machado MAAM, Cruvinel T. Effect of methylene blue-mediated antimicrobial photodynamic therapy on dentin caries microcosms. *Lasers Med Sci.*, 2018; 33(3): 479-487.
- [32] Habib IY, Burhan J, Jaladi F, Lim ChM, Usman A, Kumara NTRN, Tsang SCE, Mahadi AH. Effect of Cr doping in CeO₂ nanostructures on photocatalysis and H₂O₂ assisted methylene blue dye degradation. *Catal. Today*, 2020; 4: 1–8.
- [33] Habib IY, Zain NM, Lim CM, Usman A. Effect of Doping Rare-Earth Element on the Structural, Morphological, Optical and Photocatalytic Properties of ZnO Nanoparticles in the Degradation of Methylene Blue Dye. *IOP Conf. Series: Materials Science and Engineering*, 2021; 1127: 1–12.
- [34] Li H, Zhu M, Chen W, Xu L, Wang K. Non-light-driven reduced graphene oxide anchored TiO₂ nanocatalysts with enhanced catalytic oxidation performance. *J. Colloid Interface Sci.*, 2017; 507: 35–41.
- [35] Kim SH, Komarneni S, Heo NH. ZSM-5 and ferrierite single crystals with lower Si/Al ratios: Synthesis and single-crystal synchrotron X-ray diffraction studies. *Microporous Mesoporous Mater.*, 2011; 143(1): 243–248.

- [36] Habib IY, Kumara NTRN, Lim CM, Mahadi AH. Dynamic Light Scattering and Zeta Potential Studies of Ceria Nanoparticles. *Solid State Phenomena*, 2018; 278: 112–120.
- [37] Rahman MM, Abu-Zied BM, Asiri AM. Journal of Industrial and Engineering Chemistry Cu-loaded ZSM-5 zeolites: An ultra-sensitive phenolic sensor development for environmental safety. *J. Ind. Eng. Chem.*, 2018; 61: 304–313.
- [38] Prado NT, Oliveira LCA. Applied Catalysis B: Environmental Nanostructured niobium oxide synthesized by a new route using hydrothermal treatment: High efficiency in oxidation reactions. *Appl. Catal. B Environ.*, 2017; 205: 481–488.
- [39] Mondal SK, Saha AK, Sinha A. Removal of ciprofloxacin using modified advanced oxidation processes: Kinetics, pathways and process optimization. *J. Clean. Prod.*, 2018; 171: 1203–1214.
- [40] Wang JL, Xu LJ. Advanced oxidation processes for wastewater treatment: Formation of hydroxyl radical and application. *Crit. Rev. Environ. Sci. Technol.*, 2012; 42(3): 251–325.
- [41] Shajahan S, Arumugam P, Rajendran R, Munusamy AP. Optimization and detailed stability study on Pb doped ceria nanocubes for enhanced photodegradation of several anionic and cationic organic pollutants. *Arab. J. Chem.*, 2017; 13(1):1309-1322.
- [42] Hara J. Oxidative degradation of benzene rings using iron sulfide activated by hydrogen peroxide/ozone. *Chemosphere*, 2017; 189: 382–389.
- [43] Zhou L, Song W, Chen Z, Yin G. Degradation of organic pollutants in wastewater by bicarbonate-activated hydrogen peroxide with a supported cobalt catalyst. *Environ. Sci. Technol.*, 2013; 47(8): 3833–3839.

To whom correspondence should be addressed: I. Y. Habib, Department of Chemistry, Sa'adatu Rimi University of Education, Kano, Nigeria, E-mail: yusufishaq200@gmail.com